

# Numerical Error Extraction by Quantum Measurement Algorithm

Clément RONFAUT  
*Université Paris-Saclay  
CEA, List, F-91120  
Palaiseau, France  
0009-0006-4714-0731*

Robin OLLIVE  
*Université Paris-Saclay  
CEA, List, F-91120  
Palaiseau, France  
0009-0006-7539-363X*

Stéphane LOUISE  
*Université Paris-Saclay  
CEA, List, F-91120  
Palaiseau, France  
0000-0003-4604-6453*

**Abstract**—Important quantum algorithm routines allow the implementation of specific quantum operations (*a.k.a.* gates) by combining basic quantum circuits with an iterative structure. In this structure, the number of repetitions of the basic circuit pattern is associated to convergence parameters. This iterative structure behaves similarly to function approximation by series expansion: the higher the truncation order, the better the target gate (*i.e.* operation) approximation. The asymptotic convergence of the gate error with respect to the number of basic pattern repetitions is known. It is referred to as the query complexity. The underlying convergence law is bounded, but not in an explicit fashion. Upper bounds are generally too pessimistic to be useful in practice. The actual convergence law contains constants that depend on the joint properties of the matrix encoded by the query and the initial state vector, which are difficult to compute classically.

This paper proposes a strategy to study this convergence law and extract the associated constants from the gate (operation) approximation at different accuracy (convergence parameter) constructed directly on a Quantum Processing Unit (QPU). This protocol is called Numerical Error Extraction by Quantum Measurement Algorithm (NEEQMA). NEEQMA concepts are tested on specific instances of Quantum Signal Processing (QSP) and Hamiltonian Simulation by Trotterization. Knowing the exact convergence constants allows for selecting the smallest convergence parameters that enable reaching the required gate approximation accuracy, hence satisfying the quantum algorithm's requirements.

**Index Terms**—Approximation, Convergence, Trotter, Quantum Signal Processing (QSP), Numerical Error Extraction by Quantum Measurement Algorithm (NEEQMA)

## I. INTRODUCTION

One of the first applications proposed for quantum computers is to model the time evolution of quantum systems [1]. Mathematically, it consists in applying the Hamiltonian simulation, a unitary matrix, to the system's initial state vector [2] [3, section 4.7]. To this end, the proposed method consists of combining simpler systems' Hamiltonian simulation (known as summands) using a Product Formula (PF) [4, Section 2.3] [5]–[8]. The simplest PF consists of repeating the simpler system Hamiltonian simulation following the Lie-Trotter formula [4, Section 3.1], which is an approximation that converges geometrically toward the Hamiltonian simulation of the complete system. It can be intuitively explained using the Baker-Campbell-Hausdorff (BCH) formula [4, Section 1.1]

[2]. The parameter that controls this convergence is called the Trotter number  $n$  [4].

Another major quantum routine derived from the Hamiltonian simulation is the Quantum Phase Estimation (QPE) algorithm [9]. It produces the spectral decomposition of the time evolved Hamiltonian, where the eigenstates are intricated with the binary expression of the corresponding eigenvalue<sup>1</sup> in another quantum register. The accuracy error of the spectral decomposition is directly linked to the number of qubits in the eigenvalue readout register. It is also indirectly linked to the ability to construct the Hamiltonian simulation at a specific time:  $t = 2\pi * 2^n$  with an error on the ground-state eigenvalue smaller than  $\varepsilon$ . The number of readout qubits is a QPE convergence parameter. If a PF constructs the Hamiltonian simulation, the required number of repetitions to reach a good accuracy is a second convergence parameter. Interestingly, QPE is a subroutine of the larger Harrow–Hassidim–Lloyd algorithm (HHL) that enables block encoding of normalized functions on matrices' eigenvalues [10].

A breakthrough in quantum computing was brought with the concept of qubitization [11], which allows the extension of the QSP method to many-qubit Hamiltonians and its generalization to Quantum Singular Value Transform (QSVT) for general matrices [12], [13]. Similar to HHL, it permits the construction of a block encoding of a matrix function [13, Section II.E]. It is based on a different family of queries, known as signal operators, that are notably obtained from the matrix block encoding. This technique block encodes an arbitrary Chebyshev polynomial approximation whose degree is equal to the number of query repetitions. The polynomial coefficients are implemented through the phase angles, the parameters of the signal processing operator. The signal processing operators are inserted between the signal operators. The error in the matrix function block encoding varies in accordance with the error of the polynomial approximation of the target function evaluated on the eigenvalues. It allows one to study the QSP query complexity (for a given function) by knowing the convergence properties of a polynomial that approximates the function with a bounded error [13], [14].

<sup>1</sup>More accurately, it reads the eigenphase which are related to the eigenvalue by:  $\widehat{H_P} = \sum_j \lambda_j |\lambda_j\rangle\langle\lambda_j|$  therefore  $e^{it\widehat{H_P}} = \sum_j e^{it\lambda_j} |\lambda_j\rangle\langle\lambda_j|$ .

TABLE I  
QUANTUM ALGORITHM AND ROUTINE WITH ASSOCIATED CONVERGENCE PARAMETERS AND ERROR MODELS.

Routine /Algorithm	Convergence Parameter	Convergence law/Error Model
Trotter	Trotter number $n$	$\text{Err}(n) : (8)$
QPE	readout qubits $n$	$\varepsilon = 2^{-n}$
QSP	polynomial order $d$	$\text{Err}(d) : (18)$
$f(x)$	approx order $d$	$\varepsilon_x(d) =  f(x) - \text{poly}(d, x) $

All the previously mentioned convergence properties<sup>2</sup> and algorithms are detailed in Table I. This list of algorithms is not exhaustive but highlights how the structure of some quantum routines can be explained by analogy with polynomial function approximations Fig. 1. The convergence parameter of a quantum routine is analogous to the polynomial order, the gate (operation) error<sup>3</sup> is analogous to the truncation error  $\varepsilon$ , and the query complexity with the series rate of convergence. For practical evaluation, the initial state vector is analogous to the value on which the polynomial is evaluated. In both cases, evaluating a given state vector or a given value is necessary to study scalar convergence, rather than matrix gate error, or, by analogy, function error.

Most of the research work is interested in the asymptotic behavior of the quantum routines. Protocols that enable the production of a sufficient quality gate approximation to continue a quantum algorithm while minimizing the convergence parameters (and thus the quantum circuit figure of merit) have only recently emerged. Four articles concern PF construction with guaranteed error. Papers [15], [16] focus on long-time Hamiltonian simulation and [17] to Hamiltonian simulation as a subroutine for a QPE algorithm. A recent paper [18] also investigates free-parameters associated with QPE including the Trotter number required to find the ground state eigenvalue.

Numerical Error Extraction by Quantum Measurement Algorithm (NEEQMA) studies the convergence property of quantum routines with respect to their convergence parameters. It allows the extraction of the value of the convergence law constants (free-parameters), which are hard to compute classically. Particularly, it allows answering the question: what are the smallest parameters (shallowest circuit) that allows to reach a given accuracy in the gate approximation to construct the quantum circuit? A first section describes the general NEEQMA algorithm. The second part contains the results of NEEQMA's implementations for eigenvalues filtering by QSP and also Hamiltonian Simulation by Trotterization.

<sup>2</sup>Glossary: To the **convergence laws** are associated the **convergence law constants** that are unknown and problem-dependent. It is expressed with respect to the **convergence parameter(s)**. The convergence laws' reciprocal function (with respect to the convergence parameter) is always bounded by the **query complexity**. The **free-parameters** are associated to the **equation-to-fit**. It is derived from the error model injected in the observable equation.

<sup>3</sup>The gate error [3, section 4.5.3] is the difference between the two quantum gates:  $\widehat{E}_r(d) = \widehat{U} - \widehat{U}(d)$ . For some routines, the three matrices possess the same eigenbasis, which implies that the error convergence only behaves as the difference of the eigenvalues:  $\lambda_{E_r,i} |\lambda_i\rangle \langle \lambda_i| = |\lambda_{u,i} |\lambda_i\rangle \langle \lambda_i| - \lambda_{d,i} |\lambda_i\rangle \langle \lambda_i||$ .

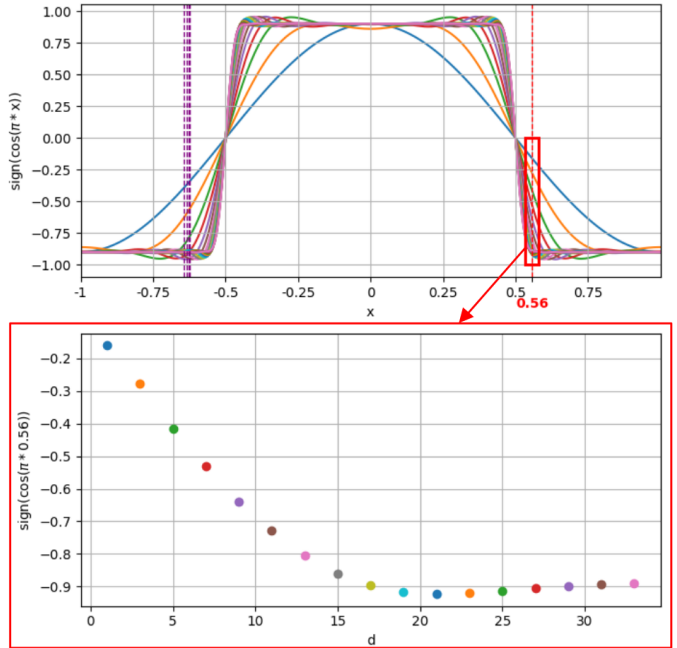


Fig. 1.  $\text{sign} \circ \cos(\pi x)$  function polynomial approximations at different orders  $d$ . The top graph represents the function approximations evaluated at many values in the  $[-1, 1]$  interval. It shows that the error fluctuates depending on the evaluation point. The bottom curve shows how the approximations converge as  $d$  increases for a chosen value equals to  $x = 0.56$  chosen for illustrative purposes; the associated error is a scalar. The purple vertical lines correspond to the eigenvalues associated with the largest  $\alpha$  values of Section III-B experiment.

## II. NUMERICAL ERROR EXTRACTION BY QUANTUM MEASUREMENT ALGORITHM

The objective of NEEQMA is, given a threshold and a quantum algorithm routine, to obtain numerical values that guarantee that the quantum routine converges below this threshold. These values facilitate the retrieval of problem-dependent constants associated with the convergence law of the quantum routine.

The key to NEEQMA is to select one (or a few) observable(s) that reflects the quantum routine convergence property when measured with respect to the convergence parameter  $d$ . By injecting the error model into the observable's equation, it is possible to derive an equation-to-fit with free-parameters. This equation-to-fit allows both for searching for the free-parameters that describe the QPU outputs and for deducing the values of the convergence law constants from the free-parameters. One method to find candidate sets of free-parameters is to use classical optimization. A choice of cost function to optimize is the difference between the observable measurement obtained thanks to the quantum circuit and the equation-to-fit at the same approximation order:

$$C(\{free_{param}\}) = \sum_{i=1}^{d_{max}} |\text{Obs}(d) - \text{FitEq}(d, \{free_{param}\})| \quad (1)$$

with  $d_{max}$  the largest value of  $d$ .

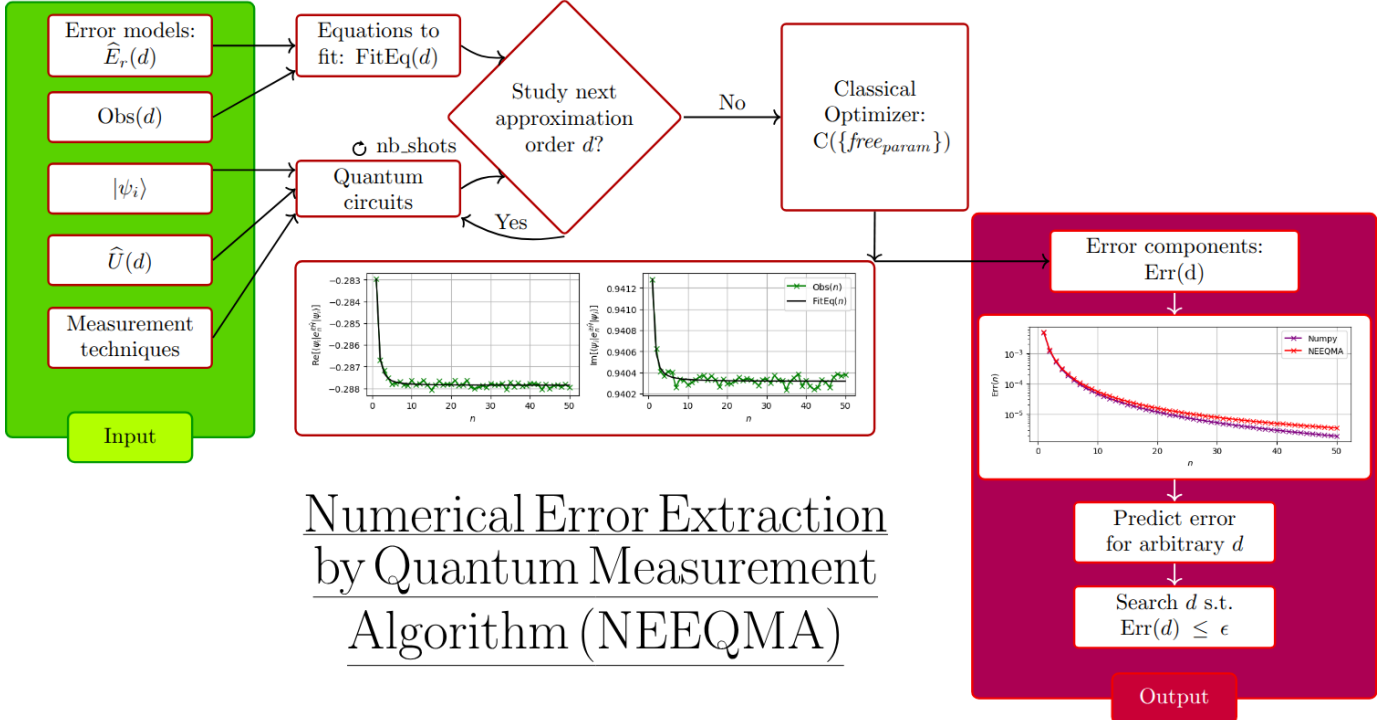


Fig. 2. NEEQMA Workflow.

Inputs needed to run the NEEQMA techniques include:

- An equation-to-fit  $\text{FitEq}(d) = \text{Obs}[\widehat{U}(d), |\psi_i\rangle]$  obtained from:
  - The gate error model which is the gate dependence in the convergence parameter:  $\widehat{U}(d) = \widehat{U} + \widehat{E}_r(d)$ .
  - Observables that can be experimentally measured on the circuit:  $\text{Obs}[\widehat{U}, |\psi_i\rangle]$ . It takes the measured quantum circuit as an input.
- Quantum circuit execution:
  - The initial state vector, from which starts the studied routine:  $|\psi_i\rangle$ .
  - The gate approximated by the routine with different values ( $d$ ) of the convergence parameter:  $\widehat{U}(d)$ .
  - The measurement circuit associated with Obs.

a) *Optional last step:* Once obtained, the convergence law constants are inserted into the error model to describe the gate error on the initial state in relation to the convergence parameters. As both the equation and constants of the convergence law are known, the curve can be extended to predict the error of a higher gate approximation order. The complete NEEQMA workflow is detailed in Fig. 2.

### III. EXPERIMENTAL REALIZATION

This section shows examples of NEEQMA's applications on two major quantum algorithms. While the error models and observables can be reused, the problem instance was selected for illustrative purposes. The cost associated with the observable sampling is not studied in these experiments.

This problem instance  $\widehat{H}_p = \sum_i \lambda_i |\lambda_i\rangle \langle \lambda_i|$  is in both cases the *LiH* molecule with an inter-nucleus distance of 2 Å. The corresponding Hamiltonian's Pauli decomposition is provided in the appendix. The normalization factor  $2|\lambda_m|$  is the norm of the largest eigenvalue and is computed classically. In practical applications, the normalization factor is chosen to be a value exceeding the magnitude of the largest eigenvalue. In both experiments, initial state vectors are the molecule Hartree-Fock (HF) states:  $|\text{HF}\rangle = |111000111000\rangle$ .

The paper appendix proposes: additional observables, details about the PF, their associated error models, as well as experimentations. The appendix also contains the QSP phase angle series and experimental details.

#### A. Hamiltonian Simulation by Trotterization

PF permits to construct the hamiltonian simulation  $e^{it\widehat{H}_p}$  given the access to  $e^{it\widehat{H}_j}$  where  $\widehat{H}_p = \sum_j \alpha_j \widehat{H}_j$ . The simplest PF is the Lie-Trotter formula:

$$e^{it\widehat{H}_p} = \lim_{n \rightarrow \infty} e_n^{it\widehat{H}_p} = \lim_{n \rightarrow \infty} \left\{ \prod_j e^{i\frac{t}{n} \alpha_j \widehat{H}_j} \right\}^n \quad (2)$$

for which the gate error is expressed using both the multiple applications of BCH formula and a Taylor series (22):

$$\begin{aligned} e^{it\widehat{H}_p} &= e_n^{i\widehat{H}_p} + \frac{\widehat{E}r_1}{n} + \frac{\widehat{E}r_2}{n^2} + \mathcal{O}(\frac{1}{n^3}) \\ &= e_n^{it\widehat{H}_p} + \widehat{E}r(n) \end{aligned} \quad (3)$$

The idea of this subsection is to model the evolution of the *LiH* molecule's electrons under the molecule's potential

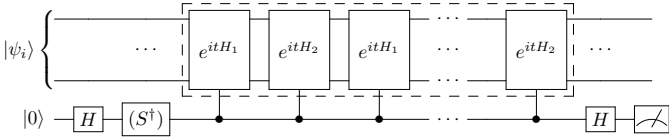


Fig. 3. Trotter plus Hadamard-test quantum circuit. Here:  $\widehat{H}_p = \widehat{H}_1 + \widehat{H}_2$ . The dashed box delimits the Trotterization routine. The  $\widehat{S}^\dagger$  gate is used to measure the imaginary part (but replaced by an identity gate when measuring the real part).

starting from the HF state. This is done for a time  $t = \frac{2\pi}{2|\lambda_m|} \times 2^5$  using the Lie-Trotter formula. This time corresponds to the simulation time needed to construct a QPE algorithm that expresses the binary result on  $n = 4$  readout qubits.

The chosen observables are the real and imaginary parts of the quantum circuit evaluated by the initial state, obtained by the Hadamard test Fig. 3:

$$\text{Obs}(n) = \left[ \text{Re}[\langle HF | e_n^{it\widehat{H}_p} | HF \rangle], \text{Im}[\langle HF | e_n^{it\widehat{H}_p} | HF \rangle] \right] \quad (4)$$

It leads to the following equations-to-fit respectively:

$$\begin{aligned} \text{FitEq}(n) &= \left[ \text{Re}[\langle HF | e_n^{it\widehat{H}_p} | HF \rangle], \text{Im}[\langle HF | e_n^{it\widehat{H}_p} | HF \rangle] \right] \\ &\simeq \left[ cr + \frac{er_1}{n} + \frac{er_2}{n^2}, \quad ci + \frac{ei_1}{n} + \frac{ei_2}{n^2} \right] \end{aligned} \quad (5)$$

with the free-parameters that are deduced:

$$\begin{aligned} cr &= \text{Re}[\langle HF | e^{it\widehat{H}_p} | HF \rangle] \\ ci &= \text{Im}[\langle HF | e^{it\widehat{H}_p} | HF \rangle] \\ er_j &= \text{Re}[\langle HF | \widehat{Er}_j | HF \rangle] \\ ei_j &= \text{Im}[\langle HF | \widehat{Er}_j | HF \rangle] \end{aligned} \quad (6)$$

The quantum circuit is similar to Fig. 3 and the curves fitted by classical optimization Fig. 4 leads to the free-parameters:

$$\begin{aligned} \tilde{cr} &\simeq 2.88 \times 10^{-1}; \quad \tilde{ci} \simeq 9.4 \times 10^{-1} \\ \tilde{er}_1 &\simeq 3.87 \times 10^{-5}; \quad \tilde{ei}_1 \simeq 9.2 \times 10^{-5} \\ \tilde{er}_2 &\simeq 4.84 \times 10^{-3}; \quad \tilde{ei}_2 \simeq 8.8 \times 10^{-4} \end{aligned} \quad (7)$$

The tilde is used to denote the value computed using NEE-QMA.

The found model constants are injected into the error model Fig. 5, which allows for expressing the error with respect to the convergence parameters:

$$\begin{aligned} \text{Err}(n) &= |\langle HF | \widehat{Er}(n) | HF \rangle| \\ &\simeq \left| \frac{e_1}{n} + \frac{e_2}{n^2} \right| \end{aligned} \quad (8)$$

with  $e_j = er_j + ie_j$ .

As the relation between the simulation time and the convergence parameters is bounded (23), it is possible to use the previous result to determine the error for an arbitrary pair

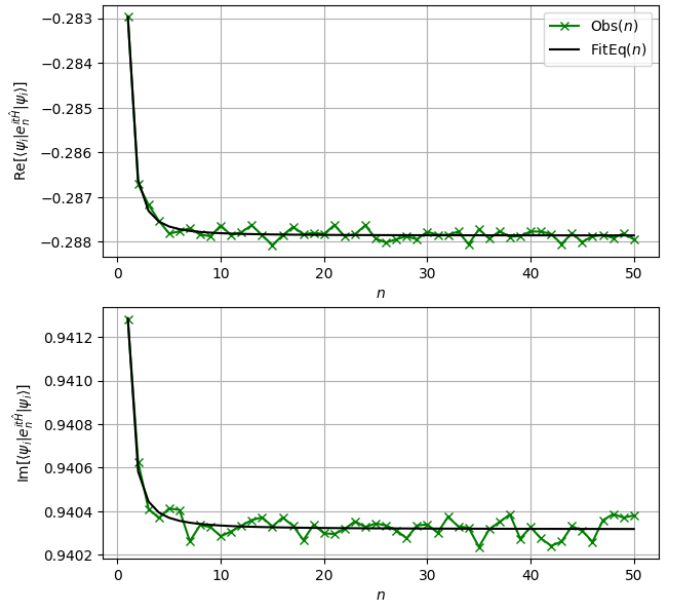


Fig. 4. Observable measurements (real and imaginary part of the Trotterized Hamiltonian simulation) at different Trotter numbers  $n$  with the associated error model, and with the free-parameters adjusted by classical optimization. This curve was computed with a Hamiltonian simulation time  $t = 1$ .

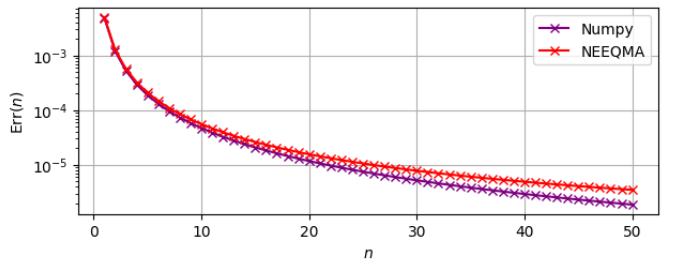


Fig. 5. Error model with the convergence law constants obtained from the quantum circuit modelling and directly from matrix calculation (using numpy) with respect to the convergence parameter  $n$  at the Hamiltonian simulation time  $t = 1$ . Note that the increasing distance between the two curves is an artefact of the graph's log scale.

of time and Trotter number Fig. 6. To this end, the time dependence of the error model is chosen as:

$$\begin{aligned} \frac{er_j(t_1)}{t_1^{j+1}} &= \frac{er_j(t_2)}{t_2^{j+1}} \\ \frac{ei_j(t_1)}{t_1^{j+1}} &= \frac{ei_j(t_2)}{t_2^{j+1}} \end{aligned} \quad (9)$$

### B. Eigenvalue Filtering by Quantum Signal Processing

This subsection explores the Intermediate Scale Quantum Computing (ISQ) algorithm for searching eigenvalues of matrices [19], [20]. It is interesting because it requires only two qubits in addition to the one that encodes the problem. It consists of doing the  $\text{Sign} \circ \cos$  function by QSP. Modifying a shift parameter on all the problem eigenvalues enables us to

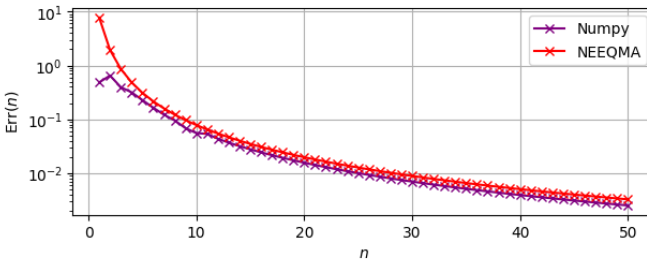


Fig. 6. Error model with the convergence laws constants obtained from the quantum circuit modelling and directly from matrix calculation (numpy) with respect to the convergence parameter  $n$  for an Hamiltonian simulation time  $t = \frac{2\pi}{2|\lambda_m|} \times 2^5$ .

perform a binary search to separate the different eigenstates based on their associated eigenvalues. At the first iteration, the search space is split between positive and negative eigenvalues, and the problem Hamiltonian is not shifted:

$$\begin{aligned} \widehat{W}_Z[\widehat{H}_p] &= \exp(it\widehat{H}_p \otimes \widehat{Z}) \\ &= \begin{bmatrix} e^{it\widehat{H}_p} & 0 \\ 0 & e^{-it\widehat{H}_p} \end{bmatrix} |HF\rangle\langle 0| \\ &= \sum_i |\lambda_i\rangle\langle\lambda_i| \otimes \begin{bmatrix} e^{it\lambda_i} & 0 \\ 0 & e^{-it\lambda_i} \end{bmatrix} |0\rangle \\ &= \sum_i |\lambda_i\rangle\langle\lambda_i| \otimes \begin{bmatrix} \cos(t\lambda_i) & -i\sin(t\lambda_i) \\ -i\sin(t\lambda_i) & \cos(t\lambda_i) \end{bmatrix} |+\rangle \end{aligned}$$

where:  $t = \frac{\pi}{2|\lambda_{\max}|}$

The following NEEQMA implementation studies the second step of the binary search. It splits the (normalized) eigenvalue space into two: the one under and the one above  $\Delta = -1/2$ . The shifted signal operator is:

$$\begin{aligned} \widehat{W}_Z[\widehat{H}_p + \Delta\widehat{I}] &= \widehat{W}_Z[\widehat{H}_p]\widehat{R}_Z(\theta = -2\delta) \\ \text{where: } \delta &= \frac{\pi}{2}\Delta \end{aligned} \quad (11)$$

The initial state is the Hartree-Fock state:  $|\psi_i\rangle = |HF\rangle \otimes |0\rangle$ . The phase angles  $\{\phi_{d,i}\}$  and polynomial coefficients  $\text{poly}(d, x)$  associated with the sign function polynomial approximation at different orders are obtained from [13], [19], [21, pyqsp code]. The associated quantum circuit Fig. 7:

$$\begin{aligned} \widehat{QSP}_Z[f] &= \prod_{m=1}^{m_\phi} \{\widehat{S}_X(\phi_m)\widehat{W}_Z\}\widehat{S}_X(\phi_0) \\ &= \sum_i |\lambda_i\rangle\langle\lambda_i| \otimes \begin{bmatrix} F(e^{it\lambda_i}) & iG(e^{it\lambda_i}) \\ iG(e^{-it\lambda_i}) & F(e^{-it\lambda_i}) \end{bmatrix} \end{aligned} \quad (12)$$

with:

$$\widehat{S}_X(\theta) = e^{i\theta\widehat{X}} = \widehat{R}_X(-2\theta) \quad (13)$$

where  $d$  is the order of the polynomial approximation of the function and  $F, G$  are real Laurent polynomials [13, APPENDIX A]. It is the convergence parameter associated

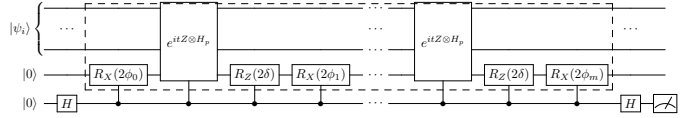


Fig. 7. QSP plus Hadamard-test quantum circuit. The dashed box delimits the QSP routine.

with the QSP routine. The chosen observable is a Hadamard test that measures the real part of the rest of the QSP quantum circuit:

$$\text{Obs}(d) = \text{Re}[\langle\psi_i| \widehat{QSP}_{\text{sign}}^d[\widehat{W}_Z] |\psi_i\rangle] \quad (14)$$

The error model with respect to the approximation order  $d$ :

$$\begin{aligned} \text{FitEq}(d, \{\lambda\}, \{\alpha_\lambda\}) &= \text{Re}[\langle\psi_i| \widehat{QSP}_{\text{sign}}^d[\widehat{W}_Z] |\psi_i\rangle] \\ &= \sum_{x \in \{\lambda\}} \alpha_x \text{Re}[F(d, e^{itx})] \\ &= \sum_{x \in \{\lambda\}} \alpha_x \text{poly}_{\text{sign}}(d, \cos(tx + \Delta)) \end{aligned} \quad (15)$$

with:  $\alpha_x = |\langle x|HF\rangle|^2 \geq 0$  and  $\sum_{x \in \{\lambda\}} \alpha_x = 1$ . If the implemented polynomials are unknown, this cost function is computable thanks to a weighted sum of one-qubit-QSP using the same series of phase angles.

The free-parameters are the eigenvalues  $\{\lambda\}$  and the norm of the projection squared of the eigenstates on the initial state  $\{\alpha_\lambda\}$ . To fit this equation, we make the strong assumption that the convergence is primarily dictated by the  $m$  eigenvalues associated with the eigenstates that have the most substantial overlap with the initial state, specifically those with the most significant  $\alpha$ . The error model constants are extracted from Fig. 8:

$$\begin{aligned} \tilde{\alpha}_{\lambda_0} &\simeq 0.7597; \quad \tilde{\lambda}_0 \simeq -1.259 \times 10^{-1} \\ \tilde{\alpha}_{\lambda_1} &\simeq 0.2289; \quad \tilde{\lambda}_1 \simeq -1.435 \times 10^{-1} \\ \tilde{\alpha}_{\lambda_2} &\simeq 0.0112; \quad \tilde{\lambda}_2 \simeq -1.207 \times 10^{-1} \end{aligned} \quad (16)$$

These can be compared to the ones obtained by diagonalization:

$$\begin{aligned} \alpha_{\lambda_0} &\simeq 0.4368; \quad \lambda_0 \simeq -1.270 \times 10^{-1} \\ \alpha_{\lambda_1} &\simeq 0.2616; \quad \lambda_1 \simeq -1.236 \times 10^{-1} \\ \alpha_{\lambda_2} &\simeq 0.1176; \quad \lambda_2 \simeq -1.331 \times 10^{-1} \end{aligned} \quad (17)$$

All the shifted eigenvalues are reported in Fig. 1.

Finally, the free-parameters are reinjected into the error model Fig. 9 to quantify the distance between the applied polynomial and the sign function:

$$\begin{aligned} \text{Err}(d) &\simeq \\ &| \sum_{x \in \{\lambda\}_m} \alpha_x (\text{sign}(\cos(\frac{\pi}{2}x)) - \text{poly}(d, \cos(\frac{\pi}{2}x))) | \end{aligned} \quad (18)$$

As the polynomial can be generated for arbitrary  $d$ , this curve can be extended to study the algorithm convergence for larger  $d$  values.

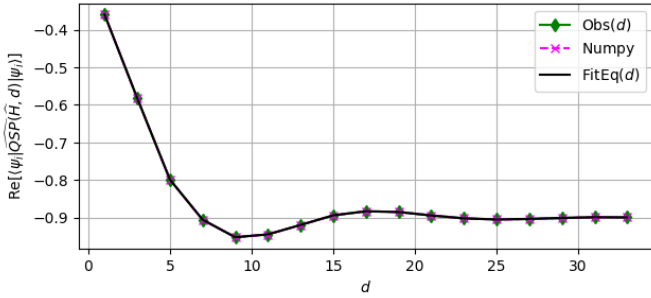


Fig. 8. Observable measurements (real part of the QSP of the Sign function) at different polynomial approximation orders  $d$  with the associated error model, with the free-parameters adjusted by classical optimization. Here  $m = 3$  and the cost function value  $C = 0.001929$ . The numpy curve is computed using the FitEq function with the eigenvalues and  $\alpha$  probabilities obtained by matrix diagonalization.

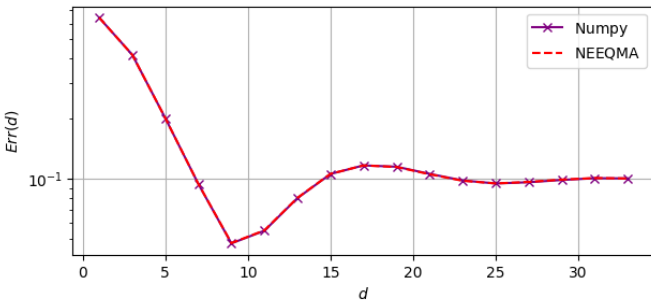


Fig. 9. Error model with the convergence laws constants obtained from the quantum circuit modelling and directly from matrix diagonalization (numpy) with respect to the approximation order  $d$ .

#### IV. CONCLUSION

This paper presents how to extract relevant information about the gate error constructed by quantum routines using carefully chosen observables directly on the QPU. Often, it is known that a quantum routine converges, but not the speed of this convergence. NEEQMA addresses this issue by expressing carefully chosen observable's values, which evolve as the gate error. We also show that when a convergence law can be derived, it allows us to extract the constants of the convergence law. Two selected routines, Lie-Trotter Hamiltonian simulation and QSP, are used to construct different quantum gates for illustrative purposes and are studied using the NEEQMA protocol. The derived equations are adaptable to other instances of these routines.

It is also interesting to mention that using a modified Hadamard test NEEQMA allows to sample arbitrary components of the error model matrix. Knowing the convergence law constants is a crucial requirement for constructing quantum routines.

#### V. FUNDING

This research work was supported in part by the French PEPR integrated project Etude de la PIle Quantique — EPIQ,

(ANR-22-PETQ-0007), it was also supported in part by the French PEPR integrated project HQI (ANR-22-PNCQ-0002).

#### VI. ACKNOWLEDGEMENT

The authors thank Pierre-Emmanuel CLET for his correction in Appendix B calculus and for providing the induction argument that proves the  $\Xi_2$  formula (24).

#### REFERENCES

- [1] R. P. Feynman, "Simulating physics with computers," *International Journal of Theoretical Physics*, vol. 21, no. 6/7, 1982.
- [2] S. Lloyd, "Universal quantum simulators," vol. 273, no. 5278, pp. 1073–1078.
- [3] M. A. Nielsen and I. L. Chuang, *Quantum Computation and Quantum Information (10th Anniversary edition)*. Cambridge University Press, 2010.
- [4] A. M. Childs, Y. Su, M. C. Tran, N. Wiebe, and S. Zhu, "A theory of trotter error," vol. 11, no. 1, p. 011020.
- [5] H. F. Trotter, "ON THE PRODUCT OF SEMI-GROUPS OF OPERATORS," p. 545.
- [6] M. Suzuki, "Generalized trotter's formula and systematic approximants of exponential operators and inner derivations with applications to many-body problems," vol. 51, no. 2, pp. 183–190.
- [7] G. H. Low, V. Kliuchnikov, and N. Wiebe, "Well-conditioned multiproduct hamiltonian simulation."
- [8] S. Zhuk, N. Robertson, and S. Bravyi, "Trotter error bounds and dynamic multi-product formulas for hamiltonian simulation."
- [9] A. Y. Kitaev, "Quantum measurements and the Abelian Stabilizer Problem," Nov. 1995. arXiv:quant-ph/9511026.
- [10] A. W. Harrow, A. Hassidim, and S. Lloyd, "Quantum algorithm for solving linear systems of equations," *Physical Review Letters*, vol. 103, p. 150502, Oct. 2009. arXiv:0811.3171 [quant-ph].
- [11] G. H. Low and I. L. Chuang, "Hamiltonian simulation by qubitization," vol. 3, p. 163.
- [12] A. Gilyén, Y. Su, G. H. Low, and N. Wiebe, "Quantum singular value transformation and beyond: exponential improvements for quantum matrix arithmetics," in *Proceedings of the 51st Annual ACM SIGACT Symposium on Theory of Computing*, pp. 193–204.
- [13] J. M. Martyn, Z. M. Rossi, A. K. Tan, and I. L. Chuang, "A grand unification of quantum algorithms," vol. 2, no. 4, p. 040203.
- [14] G. H. Low, *Quantum Signal Processing by Single-Qubit Dynamics*. PhD thesis, Department of Physics, Massachusetts Institute of Technology, 2017.
- [15] H. Zhao, M. Bukov, M. Heyl, and R. Moessner, "Making trotterization adaptive and energy-self-correcting for NISQ devices and beyond."
- [16] T. N. Ikeda, H. Kono, and K. Fujii, "Measuring trotter error and its application to precision-guaranteed hamiltonian simulations," vol. 6, no. 3, p. 033285.
- [17] S. G. Mehendale, L. A. Martínez-Martínez, P. D. Kamath, and A. F. Izmaylov, "Estimating trotter approximation errors to optimize hamiltonian partitioning for lower eigenvalue errors."
- [18] W. Sennane and J. Messud, "On the robustness of Quantum Phase Estimation to compute ground properties of many-electron systems," Jan. 2026. arXiv:2601.05788 [quant-ph].
- [19] Y. Dong, X. Meng, K. B. Whaley, and L. Lin, "Efficient phase-factor evaluation in quantum signal processing," *Physical Review A*, vol. 103, p. 042419, Apr. 2021. arXiv:2002.11649 [quant-ph].
- [20] R. OLLIVE and S. LOUISE, "Quantum Signal Processing Based Grover's Adaptive Search Oracle for High Order Unconstrained Binary Optimization Problems," in *2024 IEEE International Conference on Quantum Computing and Engineering (QCE)*, vol. 02, pp. 256–261, Sept. 2024.
- [21] R. Chao, D. Ding, A. Gilyen, C. Huang, and M. Szegedy, "Finding Angles for Quantum Signal Processing with Machine Precision," Mar. 2020. arXiv:2003.02831 [quant-ph].
- [22] A. M. Childs and N. Wiebe, "Hamiltonian simulation using linear combinations of unitary operations," vol. 12, no. 11.
- [23] D. W. Berry, A. M. Childs, R. Cleve, R. Kothari, and R. D. Somma, "Simulating hamiltonian dynamics with a truncated taylor series," vol. 114, no. 9, p. 090502.

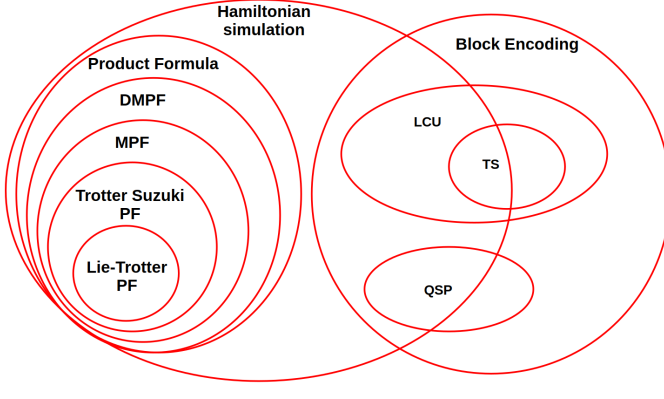


Fig. 10. Schematic diagram of the different strategies to construct Hamiltonian Simulations. When a strategy is included in a larger circle, it means this strategy is a specific instance of the larger circle strategy.

[24] R. Achilles and A. Bonfiglioli, “The early proofs of the theorem of Campbell, Baker, Hausdorff, and Dynkin,” *Archive for History of Exact Sciences*, vol. 66, pp. 295–358, May 2012.

[25] T. Giurgica-Tiron, Y. Hindy, R. LaRose, A. Mari, and W. J. Zeng, “Digital zero noise extrapolation for quantum error mitigation,” in *2020 IEEE International Conference on Quantum Computing and Engineering (QCE)*, pp. 306–316.

## APPENDIX

### A. Hamiltonian Simulation Construction

Two main families of strategies allow to construct a Hamiltonian Simulation gate (operation) on a quantum computer. They differ from the input terms needed to assemble the final gate:

- Strategies based on the problem Hamiltonian block encoding. Well adapted for Fault Tolerant Quantum Computing (FTQC): it has the best asymptotic complexity but requires many qubits. These techniques approximate the Hamiltonian simulation by truncated series expansion:
  - QSVT (and QSP) [11], [13]
  - Linear Combination of Unitaries (LCU) [22] including Truncated Taylor Series (TS) [23]
- Strategies based on the problem Hamiltonian, individual terms, or sum up the exact Hamiltonian simulation combination. The combination is achieved thanks to PF, which derives from the Trotter formula. These PF are classified by the number of parameters used to describe them:
  - Lie-Trotter PF
  - Trotter-Suzuki PF
  - Multi-PF (MPF)
  - Dynamical-Multi-PF (DMPF)

1) *Product Formula*:  $\hat{S}(t) = e^{-i\hat{H}t}$  will represent the PF approximating the evolution of the Hamiltonian. The general formula for the PF [4, eq. 15]:

$$\hat{S}(t) := \prod_{v=1}^{\Upsilon} \prod_{\gamma=1}^{\Gamma} e^{ta_{(v,\gamma)} \hat{H}_{\pi_v(\gamma)}} \quad (19)$$

‘Where  $\Upsilon$  is the number of stages of the formula, it relies on the Trotter number, when  $p = 1$ ,  $\Upsilon = 1$ , else  $\Upsilon = 2 \times 5^{\frac{p}{2}-1}$ . The permutation  $\pi_v$  controls the ordering of operator summands within stage  $v$  of the formula. The coefficients  $a_{(v,\gamma)}$  are real numbers which rely on the Trotter order and the Trotter number’ [4, p. 13].

2) *Multi product formula*: An extension to this formula introduces the Multi Product Formula (MPF) [7]:

$$\hat{S}(t) = \sum_{i=1}^n c_i \prod_{v=1}^{\Upsilon} \prod_{\gamma=1}^{\Gamma} e^{ta_{(i,v,\gamma)} \hat{H}_{\pi_v(\gamma)}} \quad (20)$$

The sum introduced by MPF allows us to modify the Trotter number at each step. Then, using a linear combination, errors introduced by each term can be approximately canceled with a proper choice of  $c_i$ , reducing the Trotter error even further.

3) *Dynamical multi product formula*: Another extension of MPF in [8], Dynamical Multi Product Formula (DMPF):

$$\hat{S}(t) = \sum_{i=1}^n c_i(t) \prod_{v=1}^{\Upsilon} \prod_{\gamma=1}^{\Gamma} e^{ta_{(i,v,\gamma)} \hat{H}_{\pi_v(\gamma)}} \quad (21)$$

In this formula, the Trotter number changes with each term of the sum, and depending on the considered interval of time. It has been demonstrated in [8] that it achieves better approximations than MPF. To make dynamic multi-product formulas resilient to uncertainty from algorithmic errors, sampling, and hardware noise, they used a minimax estimation method (Minimax MPF) [8, Section IV].

### B. Trotter Error Model Derivation

Error models associated with arbitrary PF are in general difficult to compute. Lie-Trotter PF’s error model is a specific case that admits an analytic truncated approximation. This section details this computation using this paper’s notations:

- The BCH’s formula [24]:

$$e^{\hat{C}} = e^{\hat{A}} e^{\hat{B}}$$

with  $\hat{C}(\hat{A}, \hat{B}) = \hat{A} + \hat{B} + \frac{[\hat{A}, \hat{B}]}{2} + \frac{[\hat{A}[\hat{A}, \hat{B}]] - [\hat{B}, [\hat{A}, \hat{B}]]}{12} + \dots$

Note that  $\hat{C}(\hat{A}, \hat{B}) = \hat{A} + \hat{B}$  when  $\hat{A}$  and  $\hat{B}$  commute.

- Recursive reduction of the Hamiltonian’s Hamiltonian simulation to BCH:

$$\begin{aligned} \hat{H} &= \sum_{j=0}^N \hat{H}_j \\ \Rightarrow e^{\hat{C}} &= \prod_{j=0}^N e^{t\hat{H}_j} = e^{t\hat{H}_0} \prod_{j=1}^N e^{t\hat{H}_j} \end{aligned}$$

with:

$$\begin{aligned} \hat{C} &= \hat{C}(t\hat{H}_0, \hat{C}(t\hat{H}_1, \hat{C}(t\hat{H}_2, \hat{C}(\dots, \hat{C}(t\hat{H}_{N-1}, t\hat{H}_N) \dots))) \\ &= t\hat{H} + t^2\hat{\Xi}_1 + t^3\hat{\Xi}_2 + \dots \end{aligned}$$

with:

$$\widehat{\Xi}_1 = \frac{1}{2} \sum_{j < k} [\widehat{H}_j, \widehat{H}_k]$$

$$\begin{aligned} \widehat{\Xi}_2 &= \frac{1}{12} \left( \sum_j \sum_k [\widehat{H}_j, [\widehat{H}_j, \widehat{H}_k]] \right. \\ &\quad \left. + 2 \sum_{j < k < l} ([\widehat{H}_j, [\widehat{H}_k, \widehat{H}_l]] + [\widehat{H}_l, [\widehat{H}_k, \widehat{H}_j]]) \right) \end{aligned}$$

It is based on  $e^{\widehat{A}} e^{\widehat{B}} e^{\widehat{D}} = e^{\widehat{X}} e^{\widehat{D}} = e^{\widehat{Y}}$  with  $\widehat{X} = \widehat{C}(\widehat{A}, \widehat{B})$  and  $\widehat{Y} = \widehat{C}(\widehat{X}, \widehat{D})$ .

- Trotter repetitions:

$$\left( \prod_{j=0}^N e^{\frac{t}{n} \widehat{H}_j} \right)^n = (e^{\widehat{C}(n)})^n$$

with  $\widehat{C}(n) = \frac{t}{n} \widehat{H} + (\frac{t}{n})^2 \widehat{\Xi}_1 + (\frac{t}{n})^3 \widehat{\Xi}_2 + \dots$  and

$$\begin{aligned} n\widehat{C}(n) &= t\widehat{H} + \frac{t^2}{n} \widehat{\Xi}_1 + \frac{t^3}{n^2} \widehat{\Xi}_2 + \dots \\ &= t\widehat{H} + \sum_{m=1}^{\infty} \frac{t^{m+1}}{n^m} \widehat{\Xi}_m \\ &= t\widehat{H} + \widehat{\Xi}(n, t) \end{aligned}$$

It is enough to understand that  $\lim_{n \rightarrow \infty} \widehat{\Xi}(n, t) = 0$  which implies:

$$e^{it\widehat{H}} = \lim_{n \rightarrow \infty} \left\{ \prod_j e^{i\frac{t}{n} \widehat{H}_j} \right\}^n$$

- Using Taylor series:

$$\begin{aligned} e^{t\widehat{H} + \widehat{\Xi}(n, t)} &= \sum_{k=0}^{\infty} \frac{(t\widehat{H} + \widehat{\Xi}(n, t))^k}{k!} \\ &= \sum_{k=0}^{\infty} \frac{(t\widehat{H})^k}{k!} + \sum_{k=1}^{\infty} \frac{1}{k!} \sum_{w \in \mathcal{W}_k} \prod_{w_l \in w} w_l \\ &= e^{t\widehat{H}} + \sum_{m=1}^{\infty} \frac{1}{n^m} \widehat{E}r_m \\ &\simeq e^{t\widehat{H}} + \widehat{E}r(n, t) \end{aligned} \quad (22)$$

with:

$$\mathcal{W}_k = \{t\widehat{H}, \widehat{\Xi}(n, t)\}^k \setminus \{t\widehat{H}\}^k$$

when  $m \leq 2$ ,  $\widehat{E}r_m$  is written explicitly as:

$$\begin{aligned} \widehat{E}r_1 &= \widehat{E}_{1,1} \\ \widehat{E}r_2 &= \widehat{E}_{2,1} + \widehat{E}_{1,2} \\ \widehat{E}_{m,1} &= \sum_{k=1}^{\infty} \frac{t^{k+m} \sum_{l=0}^{k-1} \widehat{H}^l \widehat{\Xi}_m \widehat{H}^{k-l-1}}{k!} \\ \widehat{E}_{m,2} &= \sum_{k=2}^{\infty} \frac{t^{k+2m}}{k!} \sum_{l+j \leq k-2} \widehat{H}^j \widehat{\Xi}_m \widehat{H}^l \widehat{\Xi}_m \widehat{H}^{k-l-j-2} \end{aligned}$$

- note that:

$$\begin{aligned} \|\widehat{E}r_1\| &\leq t^2 \|\widehat{\Xi}_1\| e^{t\|\widehat{H}\|} \\ \|\widehat{E}r_2\| &\leq t^3 (\|\widehat{\Xi}_2\| + \frac{\|\widehat{\Xi}_1\|^2}{2}) e^{t\|\widehat{H}\|} \end{aligned} \quad (23)$$

- The complete proof of  $\widehat{\Xi}_2$  formula is detailed in (24).
- $\widehat{E}r_1$  is also computed in [2, eq.(1)] and  $\widehat{\Xi}$  in [17, eq.A18].
- Note that [4, eq.(145)] propose a bound for  $\|\widehat{E}r(n = 1, t)\|$ .
- An alternative proof of the Lie-Trotter convergence is detailed in [3, section 4.7.2]. It also proposes to use the Zassenhaus formula to prove that the Trotter-Suzuki formula with the Trotter number  $n$  and Trotter order equal to 2 has faster convergence than the Lie-Trotter formula (Trotter order equal to 1).

### C. Other Observables to Measure the Error Convergence

This section details the derivation of equations-to-fit associated with other observables to run NEEQMA to construct the Hamiltonian Simulation.

These equations are derived for the Hamiltonian simulation error model truncated at order two:

$$\begin{aligned} e^{-it\widehat{H}} &= e_n^{-it\widehat{H}} - \frac{\widehat{E}r_1}{n} - \frac{\widehat{E}r_2}{n^2} + O(\frac{1}{n^3}) \\ \Leftrightarrow e_n^{-it\widehat{H}} &\approx e^{-it\widehat{H}} + \frac{\widehat{E}r_1}{n} + \frac{\widehat{E}r_2}{n^2} \end{aligned}$$

Equations-to-fit derived using the error model:

- The fidelity error<sup>4</sup> between a Trotterization of Trotter number  $n$ , and a Trotterization of Trotter number  $n + j$  with  $j \in \mathbb{N}$ :

$$\begin{aligned} &|\langle \psi_{n+j}(t) | \psi_n(t) \rangle|^2 \\ &\approx |\langle \psi_0 | (e^{-it\widehat{H}} + \frac{\widehat{E}r_1}{n+j} + \frac{\widehat{E}r_2}{(n+j)^2})^\dagger (e^{-it\widehat{H}} + \frac{\widehat{E}r_1}{n} + \frac{\widehat{E}r_2}{n^2}) | \psi_0 \rangle|^2 \\ &= |1 + \langle \psi_0 | \frac{e^{-it\widehat{H}} \widehat{E}r_1}{n} | \psi_0 \rangle + \langle \psi_0 | \frac{e^{-it\widehat{H}} \widehat{E}r_2}{n^2} | \psi_0 \rangle + \langle \psi_0 | \frac{\widehat{E}r_1^\dagger e^{-it\widehat{H}}}{n+j} | \psi_0 \rangle \\ &\quad + \langle \psi_0 | \frac{\widehat{E}r_1^\dagger \widehat{E}r_1}{n^2 + nj} | \psi_0 \rangle + \langle \psi_0 | \frac{\widehat{E}r_1^\dagger \widehat{E}r_2}{n^3 + n^2j} | \psi_0 \rangle + \langle \psi_0 | \frac{\widehat{E}r_2^\dagger e^{-it\widehat{H}}}{(n+j)^2} | \psi_0 \rangle \\ &\quad + \langle \psi_0 | \frac{\widehat{E}r_2^\dagger \widehat{E}r_1}{(n+j)^2 n} | \psi_0 \rangle + \langle \psi_0 | \frac{\widehat{E}r_2^\dagger \widehat{E}r_2}{(n+j)^2 n^2} | \psi_0 \rangle|^2 \\ &= |1 + \frac{cst_1}{n} + \frac{cst_2}{n^2} + \frac{cst_1^*}{n+j} + \frac{cst_3}{n^2 + nj} + \frac{cst_4}{n^3 + n^2j} \\ &\quad + \frac{cst_2^*}{(n+j)^2} + \frac{cst_4^*}{(n+j)^2 n} + \frac{cst_5}{(n+j)^2 n^2}|^2 \end{aligned}$$

with  $cst_1, cst_2, cst_4 \in \mathbb{C}$ ,  $cst_3, cst_5 \in \mathbb{R}$ :

$$\begin{aligned} cst_1 &= \langle \psi_0 | e^{-it\widehat{H}} \widehat{E}r_1 | \psi_0 \rangle \\ cst_2 &= \langle \psi_0 | e^{-it\widehat{H}} \widehat{E}r_2 | \psi_0 \rangle \\ cst_3 &= \langle \psi_0 | \widehat{E}r_1^\dagger \widehat{E}r_1 | \psi_0 \rangle = |\widehat{E}r_1|^2 \in \mathbb{R} \\ cst_4 &= \langle \psi_0 | \widehat{E}r_1^\dagger \widehat{E}r_2 | \psi_0 \rangle \\ cst_5 &= \langle \psi_0 | \widehat{E}r_2^\dagger \widehat{E}r_2 | \psi_0 \rangle \in \mathbb{R} \end{aligned}$$

Fig. 11 derives from NEEQMA application with this observable.

<sup>4</sup>This technique possesses similarities with the technique used in the error-mitigation Zero-Noise Extrapolation (ZNE) method [25, eq. 1]. It exploits the identity  $\widehat{U}^\dagger \widehat{U} = \widehat{I}$  to detect quantum noise arising during gate execution. Here, two different approximation orders of the Hamiltonian simulation are compared to determine if they differ. This observable is used in [16].

- Measuring the Hamiltonian energy directly by protective measurement (this observable is particularly long to compute due to the need for the expectation value of many measurement circuits):

$$\begin{aligned}
& \langle \psi_0 | (e_n^{-it\hat{H}})^\dagger \hat{H} (e_n^{-it\hat{H}}) | \psi_0 \rangle \\
& \approx \langle \psi_0 | (e^{-it\hat{H}} + \frac{\hat{E}r_1}{n} + \frac{\hat{E}r_2}{n^2})^\dagger \hat{H} (e^{-it\hat{H}} + \frac{\hat{E}r_1}{n} + \frac{\hat{E}r_2}{n^2}) | \psi_0 \rangle \\
& = \langle \psi_0 | e^{-it\hat{H}} \hat{H} e^{-it\hat{H}} | \psi_0 \rangle + \langle \psi_0 | \frac{e^{-it\hat{H}} \hat{H} \hat{E}r_1}{n} | \psi_0 \rangle \\
& + \langle \psi_0 | \frac{e^{-it\hat{H}} \hat{H} \hat{E}r_2}{n^2} | \psi_0 \rangle + \langle \psi_0 | \frac{\hat{E}r_1^\dagger \hat{H} e^{-it\hat{H}}}{n} | \psi_0 \rangle \\
& + \langle \psi_0 | \frac{\hat{E}r_1^\dagger \hat{H} \hat{E}r_1}{n^2} | \psi_0 \rangle + \langle \psi_0 | \frac{\hat{E}r_1^\dagger \hat{H} \hat{E}r_2}{n^3} | \psi_0 \rangle \\
& + \langle \psi_0 | \frac{\hat{E}r_2^\dagger \hat{H} e^{-it\hat{H}}}{n^2} | \psi_0 \rangle + \langle \psi_0 | \frac{\hat{E}r_2^\dagger \hat{H} \hat{E}r_1}{n^3} | \psi_0 \rangle + \langle \psi_0 | \frac{\hat{E}r_2^\dagger \hat{H} \hat{E}r_2}{n^4} | \psi_0 \rangle \\
& = cst_1 + \frac{cst_2}{n^2} + \frac{cst_3}{n^2} + \frac{cst_2^*}{n} + \frac{cst_4}{n^2} + \frac{cst_5}{n^3} + \frac{cst_3^*}{n^2} \\
& + \frac{cst_5^*}{n^3} + \frac{cst_6}{n^4} \\
& = cst_1 + \frac{2}{n} \text{Re}[cst_2] + \frac{2}{n^2} \text{Re}[cst_3] + \frac{cst_4}{n^2} + \frac{2}{n^3} \text{Re}[cst_5] + \frac{cst_6}{n^4}
\end{aligned}$$

with  $cst_1, cst_4, cst_6 \in \mathbb{R}, cst_2, cst_3, cst_5 \in \mathbb{C}$ :

$$\begin{aligned}
cst_1 &= \langle \psi_0 | e^{-it\hat{H}} \hat{H} e^{-it\hat{H}} | \psi_0 \rangle = \langle \psi_0 | \hat{H} | \psi_0 \rangle \\
cst_2 &= \langle \psi_0 | e^{-it\hat{H}} \hat{H} \hat{E}r_1 | \psi_0 \rangle \\
cst_3 &= \langle \psi_0 | e^{-it\hat{H}} \hat{H} \hat{E}r_2 | \psi_0 \rangle \\
cst_4 &= \langle \psi_0 | \hat{E}r_1^\dagger \hat{H} \hat{E}r_1 | \psi_0 \rangle = |\hat{E}r_1|^2 \langle Er_1 | \hat{H} | Er_1 \rangle \in \mathbb{R} \\
cst_5 &= \langle \psi_0 | \hat{E}r_1^\dagger \hat{H} \hat{E}r_2 | \psi_0 \rangle \\
cst_6 &= \langle \psi_0 | \hat{E}r_2^\dagger \hat{H} \hat{E}r_2 | \psi_0 \rangle
\end{aligned}$$

Fig. 12 derives from NEEQMA application with this observable. This observable is used in [15].

- The phase is a particularly interesting observable for reconstructing the convergence of the error, as it allows for the isolation of its real and imaginary parts thanks to the Hadamard test. On top of giving us direct information on real and imaginary parts of Trotter error, it only needs to evaluate one single quantum circuit:

$$\begin{aligned}
& |\langle \psi_i | e_n^{-it\hat{H}} | \psi_i \rangle|^2 \\
& \approx |\langle \psi_i | e^{-it\hat{H}} + \frac{\hat{E}r_1}{n} + \frac{\hat{E}r_2}{n^2} | \psi_i \rangle|^2 \\
& = |\langle \psi_i | e^{-it\hat{H}} | \psi_i \rangle + \langle \psi_i | \frac{\hat{E}r_1}{n} | \psi_i \rangle + \langle \psi_i | \frac{\hat{E}r_2}{n^2} | \psi_i \rangle|^2 \\
& = |cst_1 + \frac{cst_2}{n} + \frac{cst_3}{n^2}|^2
\end{aligned}$$

with  $cst_1 \in \mathbb{R}, cst_2, cst_3 \in \mathbb{C}$ :

$$\begin{aligned}
cst_1 &= \langle \psi_i | e^{-it\hat{H}} | \psi_i \rangle \\
cst_2 &= \langle \psi_i | \hat{E}r_1 | \psi_i \rangle \\
cst_3 &= \langle \psi_i | \hat{E}r_2 | \psi_i \rangle
\end{aligned}$$

Fig. 13 derives from NEEQMA application with this observable.

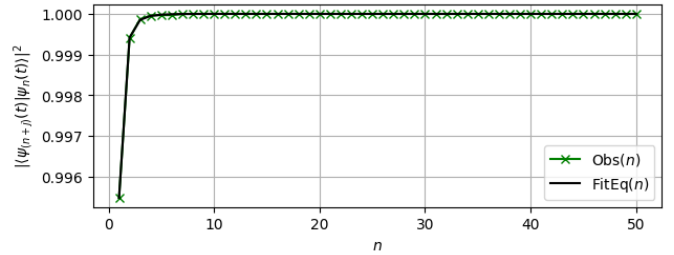


Fig. 11. Observable measurement (fidelity between the Trotterized Hamiltonian simulation at trotter number  $n$  and  $(n + j)$ ,  $j = 1$ ) at different Trotter numbers  $n$  with the associated error model, with the free-parameters adjusted by classical optimization. This curve was computed at Hamiltonian simulation's time  $t = 1$ .

Real part:

$$\begin{aligned}
& \text{Re}[\langle \psi_i | e_n^{-it\hat{H}} | \psi_i \rangle] \\
& \approx \text{Re}[\langle \psi_i | e^{-it\hat{H}} + \frac{\hat{E}r_1}{n} + \frac{\hat{E}r_2}{n^2} | \psi_i \rangle] \\
& = \text{Re}[\langle \psi_i | e^{-it\hat{H}} | \psi_i \rangle] + \text{Re}[\langle \psi_i | \frac{\hat{E}r_1}{n} | \psi_i \rangle] \\
& \quad + \text{Re}[\langle \psi_i | \frac{\hat{E}r_2}{n^2} | \psi_i \rangle] \\
& = cst_1 + \frac{cst_2}{n} + \frac{cst_3}{n^2}
\end{aligned}$$

with  $cst_1, cst_2, cst_3 \in \mathbb{R}$ :

$$\begin{aligned}
cst_1 &= \text{Re}[\langle \psi_i | e^{-it\hat{H}} | \psi_i \rangle] \\
cst_2 &= \text{Re}[\langle \psi_i | \hat{E}r_1 | \psi_i \rangle] \\
cst_3 &= \text{Re}[\langle \psi_i | \hat{E}r_2 | \psi_i \rangle]
\end{aligned}$$

Fig. 4 derives from NEEQMA application with this observable.

Imaginary part:

$$\begin{aligned}
& \text{Im}[\langle \psi_i | e_n^{-it\hat{H}} | \psi_i \rangle] \\
& \approx \text{Im}[\langle \psi_i | e^{-it\hat{H}} + \frac{\hat{E}r_1}{n} + \frac{\hat{E}r_2}{n^2} | \psi_i \rangle] \\
& = \text{Im}[\langle \psi_i | e^{-it\hat{H}} | \psi_i \rangle] + \text{Im}[\langle \psi_i | \frac{\hat{E}r_1}{n} | \psi_i \rangle] \\
& \quad + \text{Im}[\langle \psi_i | \frac{\hat{E}r_2}{n^2} | \psi_i \rangle] \\
& = cst_1 + \frac{cst_2}{n} + \frac{cst_3}{n^2}
\end{aligned}$$

with  $cst_1, cst_2, cst_3 \in \mathbb{R}$ :

$$\begin{aligned}
cst_1 &= \text{Im}[\langle \psi_i | e^{-it\hat{H}} | \psi_i \rangle] \\
cst_2 &= \text{Im}[\langle \psi_i | \hat{E}r_1 | \psi_i \rangle] \\
cst_3 &= \text{Im}[\langle \psi_i | \hat{E}r_2 | \psi_i \rangle]
\end{aligned}$$

Fig. 4 derives from NEEQMA application with this observable.

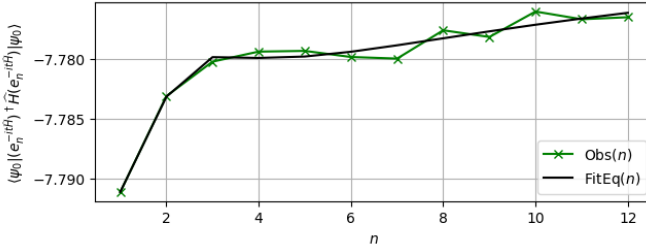


Fig. 12. Observable measurement (energy of the Trotterized Hamiltonian simulation) at different Trotter numbers  $n$  with the associated error model, with the free-parameters adjusted by classical optimization. This curve was computed at Hamiltonian simulation's time  $t = 1$ .

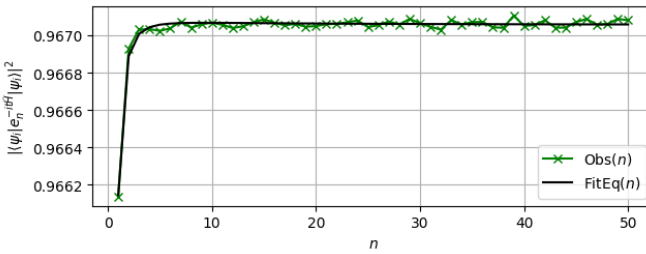


Fig. 13. Observable measurement (phase of the Trotterized Hamiltonian simulation) at different Trotter numbers  $n$  with the associated error model, with the free-parameters adjusted by classical optimization. This curve was computed at Hamiltonian simulation's time  $t = 1$ .

#### D. Related Work

This section gives an overview of the related work [16] previously mentioned. In order to underline the differences with our approach, [16]'s algorithm: Trotter24 is presented using a workflow with a structure similar to the one used for NEEQMA Fig. 2.

Trotter24 aims at realizing the Hamiltonian simulation under the constraint of a defined accuracy at each time step. The way the authors proceed to reduce their Trotter error is by starting with the simulation of a chosen Hamiltonian on a small time step and estimate the Trotter error (the estimated observable is the fidelity, as described in Section C). If the error is greater than  $\epsilon$  (desired accuracy), Trotter24 restarts the simulation with an even smaller time step until the error is less than  $\epsilon$ . From there, it repeats the process until it has completely simulated the Hamiltonian (when the sum of the saved time steps reaches the time  $t$ ). Since the sizes of the selected time steps can be different, this iterative adaptive algorithm proposal cannot be considered equivalent to working with a Trotter number.

This section presents the details of the algorithm realized in the related work [16] using a workflow Fig. 14. The Workflow description follows:

- As inputs it is required to have an initial state  $|\psi_i\rangle$ , a total simulation time  $t_{fin}$ , a problem  $\hat{H}$ , a time step error bound  $\epsilon$ , a constant  $C \in [0, 1]$  used to update the time step duration, an *initial time step duration*  $\delta t_0$ .
- It starts by creating  $U_{list}$  to save time steps that

respect the accuracy constraint  $\epsilon$ , it also fixes the *actual time step duration*  $\delta_t$  to  $\delta t_0$  and the *studied time* to 0.

- After initializing  $|\psi_i\rangle$  in a quantum circuit, it applies a series of Trotter gates on  $\hat{H}$  with order 2 for every time steps saved in  $U_{list}$  (when  $U_{list}$  is empty, it simply skips this step).
- Using the time step  $\delta_t$ , it applies a Trotter gate of order 2, followed by an adjoint Trotter gate of order 4 on the same time step  $\delta_t$  and on the same Hamiltonian  $\hat{H}$ .
- To cancel out unnecessary terms (time steps saved in  $U_{list}$ ), it applies a series of adjoints Trotter gates on  $\hat{H}$  with order 2 for every time steps saved in  $U_{list}$  (when  $U_{list}$  is empty it simply skips this step). It then measures all qubits and calculates the fidelity error.
- If the fidelity error is greater than  $\epsilon$ , it restarts the process with a lower time step:  $\delta_t \leftarrow C\delta_t$ .
- If the fidelity error is lower than  $\epsilon$ , it saves  $\delta_t$  in  $U_{list}$ , increases  $t_{studied}$  with  $\delta_t$ .
- If the total time  $t_{fin}$  is not yet reached, it starts again the quantum circuit, this time using the updated  $U_{list}$ .
- If the total time  $t_{fin}$  is reached, it outputs  $U_{list}$  containing all time step durations required to perform Trotterization on a given time  $t_{fin}$  while respecting the constraint given by  $\epsilon$  on any time steps.
- To check whether the simulation is accurate, the authors measure in the Z-basis at each time step, the x-magnetization  $\widehat{m}_x \equiv \frac{1}{L} \sum_{j=1}^L \widehat{\sigma}_j^x$  of the Trotterization shown on Fig. 14 (a), since the x-magnetization evolution follows a natural and expected sinusoidal curve, it shows an accurate simulation.
- Finally, the authors have plotted the accumulated error over the whole simulation (point curves) represented by Fig. 14 (b). To calculate the accumulated error, Trotter24 initializes  $|\psi_i\rangle$  in a quantum circuit, and apply a series of Trotter gates on  $\hat{H}$  with order 2 for every time steps saved in  $U_{list}$  followed by a series of adjoints Trotter gates on  $\hat{H}$  with order 4 for every time steps saved in the reversed  $U_{list}$ . The upper bound curves are calculated assuming fidelity errors equal  $\epsilon$  on every time steps in  $U_{list}$ , this can be achieved when  $C \approx 1$ .

#### E. Experimental Details

All experiments were realized using quantum circuits with a number of shots equal to  $10^5$ , except the experiments to measure  $Obs(n)$  in Fig. 13 and Fig. 4 where we used  $10^8$  shots.

1) *Optimizer Parameters*: For the Hamiltonian Simulation experiment, we have used the `curve_fit` method from the `scipy.optimize` package. For the QSP experiment, we have used the `cobyla` method from the `scipy.optimize` package.

2) *Sign Function Phase Angles*: Each list contains a size associated with a different degree. These lists are obtained thanks to the prompt

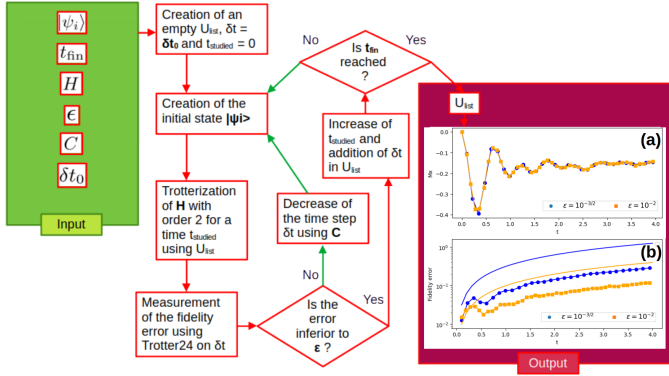


Fig. 14. Trotter24 workflow [16]. (a) Dynamics of x-magnetization density calculated by fidelity-based Trotter24 for tolerance  $\epsilon = 10^{-3/2}$  (circle) and  $10^{-2}$  (square). (a) is a reproduction of [16, fig 2.a]. (b) Fidelity errors in the simulation presented in (a). Solid curves show upper bounds. Blue (orange) points and curve correspond to  $\epsilon = 10^{-3/2}$  ( $10^{-2}$ ). (b) is a reproduction of [16, fig 2.b].

```
'pyqsp --plot --polyargs=1,d --plot-real-only
--polynname poly_sign poly --return-angles'
```

in the [13], [19], [21, pyqsp code] package, all the raw phase angles are contained in the associated folder

```
'sign_function_qsp_phase_angle_from_pyqsp.txt'.
```

3) *Hamiltonian*: Utilized normalization factor (obtained from numpy):  $|\lambda_m| = 8.654853588861483$ . *LiH* Hamiltonian Pauli-string decomposition is contained in the associated file named `lih_2a.txt`.

Starting with: 
$$\begin{cases} \widehat{C}(\widehat{A}, \widehat{B}) = \widehat{A} + \widehat{B} + \frac{[\widehat{A}, \widehat{B}]}{2} + \frac{[\widehat{A}[\widehat{A}, \widehat{B}]] + [\widehat{B}, [\widehat{B}, \widehat{A}]]}{12} \\ \widehat{B} = t \widehat{H}_{N+1} \\ \widehat{A}_N = t \sum_{j=0}^N \widehat{H}_j + t^2 \widehat{\Xi}_{1,N} + t^3 \widehat{\Xi}_{2,N} + \mathcal{O}(t^4) \end{cases}$$

we want to shows that: 
$$\begin{cases} \widehat{\Xi}_{1,N} = \frac{1}{2} \sum_{0 \leq j < k \leq N} [\widehat{H}_j, \widehat{H}_k] \\ \widehat{\Xi}_{2,N} = \frac{1}{12} (\sum_{j=0}^N \sum_{k=0}^N [\widehat{H}_j, [\widehat{H}_j, \widehat{H}_k]] + 2 \sum_{0 \leq j < k < l \leq N} ([\widehat{H}_j, [\widehat{H}_k, \widehat{H}_l]] + [\widehat{H}_l, [\widehat{H}_k, \widehat{H}_j]])) \end{cases}$$

For  $N = 0$ :  $\widehat{A}_0 = t \sum_{j=0}^0 \widehat{H}_j + t^2 \widehat{\Xi}_{1,N=0} + t^3 \widehat{\Xi}_{2,N=0} = t \widehat{H}_0$  which is true.

Recurrence:  $\widehat{A}_{N+1} = \widehat{C}(\widehat{A}_N, \widehat{B})$

$$\begin{aligned} &= t \sum_{j=0}^N \widehat{H}_j + t^2 \widehat{\Xi}_{1,N} + t^3 \widehat{\Xi}_{2,N} + t \widehat{H}_{N+1} + \frac{[(t \sum_{j=0}^N \widehat{H}_j + t^2 \widehat{\Xi}_{1,N}), t \widehat{H}_{N+1}]}{2} \\ &\quad + \frac{[t \sum_{j=0}^N \widehat{H}_j [t \sum_{j=0}^N \widehat{H}_j, t \widehat{H}_{N+1}]] + [t \widehat{H}_{N+1}, [t \widehat{H}_{N+1}, t \sum_{j=0}^N \widehat{H}_j]]}{12} + \mathcal{O}(t^4) \\ &= t \sum_{j=0}^{N+1} \widehat{H}_j + t^2 \widehat{M}_1 + t^3 \widehat{M}_2 + \mathcal{O}(t^4) \end{aligned}$$

with:  $\widehat{M}_1 = \widehat{\Xi}_{1,N} + \frac{[\sum_{j=0}^N \widehat{H}_j, \widehat{H}_{N+1}]}{2} = \sum_{0 \leq j < k \leq N+1} \frac{[\widehat{H}_j, \widehat{H}_k]}{2} = \widehat{\Xi}_{1,N+1}$

and:  $\widehat{M}_2 = \widehat{\Xi}_{2,N} + \sum_{0 \leq j < k \leq N} \frac{[[\widehat{H}_j, \widehat{H}_k], \widehat{H}_{N+1}]}{4} + \frac{\sum_{j=0}^N \sum_{k=0}^N [\widehat{H}_j [\widehat{H}_k, \widehat{H}_{N+1}]] + \sum_{j=0}^N [\widehat{H}_{N+1}, [\widehat{H}_{N+1}, \widehat{H}_j]]}{12}$

$$\begin{aligned} &= \frac{1}{12} (\sum_{j=0}^N \sum_{k=0}^N [\widehat{H}_j, [\widehat{H}_j, \widehat{H}_k]] + 2 \sum_{0 \leq j < k < l \leq N} ([\widehat{H}_j, [\widehat{H}_k, \widehat{H}_l]] + [\widehat{H}_l, [\widehat{H}_k, \widehat{H}_j]])) \\ &\quad + 3 \sum_{0 \leq j < k \leq N} [[\widehat{H}_j, \widehat{H}_k], \widehat{H}_{N+1}] + \sum_{j=0}^N \sum_{k=0}^N [\widehat{H}_j [\widehat{H}_k, \widehat{H}_{N+1}]] + \sum_{j=0}^N [\widehat{H}_{N+1}, [\widehat{H}_{N+1}, \widehat{H}_j]]) \end{aligned}$$

Using:

$$\begin{aligned} (*) \sum_{j=0}^N \sum_{k=0}^N [\widehat{H}_j [\widehat{H}_k, \widehat{H}_{N+1}]] &= \sum_{j=0}^N [\widehat{H}_j [\widehat{H}_j, \widehat{H}_{N+1}]] + \sum_{0 \leq j < k \leq N} ([\widehat{H}_j [\widehat{H}_k, \widehat{H}_{N+1}]] + [\widehat{H}_k [\widehat{H}_j, \widehat{H}_{N+1}]]) \\ \Rightarrow \widehat{M}_2 &= \frac{1}{12} (\sum_{j=0}^{N+1} \sum_{k=0}^{N+1} [\widehat{H}_j, [\widehat{H}_j, \widehat{H}_k]] + 2 \sum_{0 \leq j < k < l \leq N} ([\widehat{H}_j, [\widehat{H}_k, \widehat{H}_l]] + [\widehat{H}_l, [\widehat{H}_k, \widehat{H}_j]])) \\ &\quad + 3 \sum_{0 \leq j < k \leq N} [\widehat{H}_{N+1}, [\widehat{H}_k, \widehat{H}_j]] + \sum_{0 \leq j < k \leq N} ([\widehat{H}_j [\widehat{H}_k, \widehat{H}_{N+1}]] + [\widehat{H}_k [\widehat{H}_j, \widehat{H}_{N+1}]])) \end{aligned}$$

Using:

$$\begin{aligned} (**) 0 &= [k, [j, l]] + [j, [l, k]] + [l, [k, j]] \\ \Rightarrow \widehat{M}_2 &= \frac{1}{12} (\sum_{j=0}^{N+1} \sum_{k=0}^{N+1} [\widehat{H}_j, [\widehat{H}_j, \widehat{H}_k]] + 2 \sum_{0 \leq j < k < l \leq N} ([\widehat{H}_j, [\widehat{H}_k, \widehat{H}_l]] + [\widehat{H}_l, [\widehat{H}_k, \widehat{H}_j]])) \\ &\quad + 2 \sum_{0 \leq j < k \leq N} ([\widehat{H}_{N+1}, [\widehat{H}_k, \widehat{H}_j]] + [\widehat{H}_j [\widehat{H}_k, \widehat{H}_{N+1}]])) \\ &= \widehat{\Xi}_{2,N+1} \end{aligned} \tag{24}$$

Fig. 15.  $\widehat{\Xi}$  formula proof by induction.